LRP 445/91 December 1991

RESISTIVE TOROIDAL STABILITY OF INTERNAL KINK MODES IN CIRCULAR AND SHAPED TOKAMAKS

A. Bondeson, G. Vlad, H. Lütjens

Submitted to Physics of Fluids B

Resistive toroidal stability of internal kink modes in circular and shaped tokamaks

A. Bondeson[a], G. Vlad[b] and H. Lütjens[a]

[a]Centre de Recherches en Physique des Plasmas,
Association Euratom - Confédération Suisse, Ecole Polytechnique Fédérale de Lausanne,
21 Av. des Bains, CH-1007 Lausanne, Switzerland

[b]Associazione Euratom - ENEA sulla Fusione, C.R.E. Frascati,
C.P. 65-00044 - Frascati, Rome, Italy

Abstract: The linear resistive magnetohydrodynamical (MHD) stability of the n = 1 internal kink mode in tokamaks is studied by toroidal computations. The stabilizing influence of small aspect ratio [Holmes, et al., Phys. Fluids **B1**, 788 (1989)] is confirmed, but it is found that shaping of the cross section influences the internal kink mode significantly. For finite pressure and small resistivity, curvature effects at the q = 1 surface make the stability sensitively dependent on shape, and ellipticity (including JET shape) is destabilizing. Only a very restricted set of finite pressure equilibria is completely stable for $q_0 < 1$. A typical result is that the resistive kink mode is slowed down by toroidal effects to a weak tearing/resistive interchange mode. It is suggested that weak resistive instabilities are stabilized during the ramp phase of the sawteeth by effects not included in the linear resistive MHD model. Possible mechanisms for triggering a sawtooth crash are discussed.

I. Introduction

The stability properties of the internal kink mode are of interest for understanding the sawtooth oscillations in tokamaks. Kadomtsev[1] suggested that the sawteeth are triggered by an internal kink mode of toroidal mode number n = 1 becoming unstable when the central safety factor q_0 falls below unity, and that the nonlinear evolution of this instability leads to complete resistive reconnection. Bussac et al[2,3] studied the stability of the internal kink by means of a large aspect ratio expansion. In contrast with the cylindrical result, they found that the *ideal* internal kink mode is stable in toroidal geometry when the poloidal beta at the q = 1 surface is below a threshold value (typically between 0.1 and 0.3, depending on the current profile).[2] Similarly, the *resistive* mode is slowed down from the resistive kink behavior (ideally marginal with $\Delta' = \infty$) at infinite aspect ratio and small pressure to a weaker tearing instability ($0 < \Delta' < \infty$) at finite aspect ratio.[3] Recent experimental investigations show a safety factor in the center of tokamaks well below unity[4,5] and indicate that it remains so even after the sawtooth crash,[6,7] while other measurements have found q-profiles that are flat and close to unity in the central region.[8,9] It has been found computationally that the resistive internal kink can be linearly stable if the shear at the q = 1 surface is weak.[4,10] This holds, in particular, when q_0 is well below unity, provided the shear is locally reduced at the q = 1 surface, i.e., for current profile with "shoulders" at q = 1, as found on the TEXTOR tokamak.[4] In addition to profile effects, the internal kink mode can be stabilized by the presence of hot particles.[11,12] The sawtooth oscillations have been stabilized in discharges with $q_0 < 1$, and the stabilization has been attributed either to current profile modification[13] or to hot particle effects.[14] It is well known that non-MHD effects can strongly modify the stability of the internal kink mode.[15-17] Nevertheless, it is of interest to understand its stability properties within the simplest theoretical framework of resistive MHD. This is the goal of the present paper.

Even within magnetohydrodynamics, the internal kink mode is sensitive to a large number of parameters.[10,18] Here, we examine the effects of aspect ratio, shaping of the cross section, current profiles, pressure and wall separation. Growth rates of the n = 1 mode are computed numerically from the full, resistive, compressible MHD equations for two-dimensional, static, toroidal equilibria, using the recently developed, toroidal, resistive code MARS[19] and the equilibrium code CHEASE.[20] Several of the numerical results can be understood analytically by considering the resistive and ideal interchange criteria, which play important roles for the linear stability of the internal kink. For very low pressure and circular cross section, our results confirm those of Holmes et al.[10] Stability is favored by small aspect ratio, low shear at q = 1, and low q_0. However, even slight pressure severely restricts the region of *complete* resistive MHD stability with $q_0 < 1$. This is due in part to violation of the resistive interchange criterion. A typical result, when pressure and shape effects are taken into account, is that the mode is slowed down by toroidal effects and is turned into a weak tearing/resistive interchange mode at small resistivities. Elliptic shaping renders pressure gradients considerably more destabilizing than for circular flux surfaces by violation of the resistive interchange criterion.

II. Dependence on aspect ratio, shaping and wall separation

II.A Specification of equilibria

We first study the effects of aspect ratio, shear at the q = 1 surface and wall separation for different cross sections at zero pressure. The plasma-vacuum boundary is prescribed according to the INTOR formula:

$$R = R_0 + a\cos(\theta + \delta \sin\theta) \quad , \qquad Z = a\,\kappa \sin\theta \quad , \tag{1}$$

where a is the minor radius, R_0 the major radius of the geometrical center, κ the elongation and δ the triangularity. For this study, we have chosen three particular shapes: circular (κ =1, δ = 0), elliptic (κ = 1.7, δ = 0) and JET shape (κ = 1.7, δ = 0.3).

The current profiles are specified by the surface averaged toroidal current density,

$$I^* \equiv \frac{\int j_\phi\,(J/R)\,d\chi}{\int (J/R)\,d\chi} \quad , \tag{2}$$

[where J is the Jacobian for the transformation from flux coordinates (ψ, χ, ϕ) to Cartesian coordinates] as a function of the normalized poloidal flux ψ/ψ_{axis}. $I^*(\psi/\psi_{axis})$ is prescribed except for a multiplicative factor that is adjusted to specify the q = 1 radius.

We first consider two current profiles that give a rather uniform and low shear inside a certain radius $\rho = \rho_p \approx 0.44$ [where $\rho(\psi) \equiv (V(\psi)/V_{tot})^{1/2}$ is a normalized minor radius and $V(\psi)$ denotes the volume enclosed by a flux surface ψ = constant]. Outside this radius, the shear rises sharply. For $\rho < \rho_p$, I* is taken to be a quadratic polynomial in $(\psi/\psi_{axis})^{1/2}$ with zero slope at $\rho = \rho_p$ but nonzero slope at the origin. In studying the aspect ratio dependence, we hold the q = 1 radius fixed at $\rho \approx 0.40$, slightly inside the "knee" of the q-profile at $\rho = \rho_p$. Two different values of the central shear have been chosen, such that

$$s = \frac{\rho}{q}\,\frac{dq}{d\rho} \tag{3}$$

at q = 1 is about 0.04 and 0.07, and $q_0 \approx 0.935$ and 0.88 respectively. The shear varies slightly with the aspect ratio and the shape. Figure 1 shows $I^*(\rho)$, $q(\rho)$ and $s(\rho)$ for the circular equilibrium with low central shear, $s_{q=1} = 0.04$, and aspect ratio $A = R_0/a = 3$.

For simplicity, the mass density and resistivity η are taken constant in space. The resistivity is indicated by the Lundquist number $S = \tau_r/\tau_A$, where $\tau_r = \mu_0 a^2/\eta$ is the resistive time connected with the minor radius and $\tau_A = R_0/v_{A0}$ is the toroidal Alfvén time. The growth rates are normalized with respect to τ_A.

II.B Fixed boundary results for zero pressure

At low pressure, the resistive internal kink mode is stabilized by small aspect ratio and weak shear at the q = 1 surface.[10] This is exemplified in Fig. 2, which shows the fixed boundary growth rates of the resistive kink mode vs. the inverse aspect ratio $\varepsilon \equiv a/R_0$ for the three different cross sections under study (circle, ellipse and JET shape) and the two different values of central shear. The Lundquist number is $S = 10^6$. Figure 2 shows that not only shear but also shaping is important.

The shaping effects are more significant at large aspect ratio. For example, the elliptic case ($\kappa = 1.7$, $\delta = 0$) shows strong instability as the aspect ratio increases. The destabilization by ellipticity has been analyzed for ideal modes at large aspect ratio.[21,22] It is connected to contributions proportional to $(\kappa-1)^2$ in the normalized potential energy $\delta W/a^2$. The destabilizing elliptic term competes with the $O(\varepsilon^2)$ stabilizing toroidal contribution.[2] At sufficiently large aspect ratio, the shaping terms dominate over the toroidal terms and an elliptical equilibrium with $q_0 < 1$ is *ideally* unstable at sufficiently large aspect ratio. As shown by Fig. 2, the resistive internal mode is significantly destabilized by an ellipticity of $\kappa = 1.7$ for aspect ratios of interest. However, a triangularity of $\delta = 0.3$, in combination with the same ellipticity, improves stability compared to the circle. This can be explained in terms of stabilizing terms of order $\varepsilon(\kappa-1)\delta$ and δ^2 in $\delta W/a^2$. These shaping terms become significant at large aspect ratio, as shown by Fig. 2.

At low aspect ratio, the toroidal effects tend to dominate over the shaping effects and the growth rates of the internal kink mode are significantly reduced. Figure 2 shows that, for the low shear profile, the three shapes are stabilized at roughly the same aspect ratio, $A = R_0/a \approx 3$. For the high shear profile, the circular and JET-shaped equilibria are stable for A less than about 1.5 and 1.8 respectively. By contrast, the elliptic cross section is never completely stabilized, and the growth rate even increases for $\varepsilon > 0.6$ [as a consequence of destabilizing terms of order $(\kappa-1)\varepsilon^2$ in $\delta W/a^2$]. Thus, ellipticity alone is destabilizing, but a combination of triangularity and ellipticity is favorable for stability also at low aspect ratio.

To summarize the results of Fig. 2 for the fixed boundary internal kink at *zero pressure*: toroidicity and weak shear at the q = 1 surface are stabilizing, ellipticity is destabilizing, but a combination of ellipticity and sufficient triangularity is more stable than a circular equilibrium.

II.C Free boundary results for zero pressure

Next, we consider the effects of a free boundary. Figure 3 a shows the growth rate of the n = 1 mode at $S = 10^6$ for a circular zero beta equilibrium (the case of weak central shear in Fig. 2). One curve gives the result for a fixed boundary and the two others apply to free boundary modes with a conducting wall placed at a radius of b = 1.2a.

At large aspect ratio, the two free boundary modes correspond in an unambiguous way to their cylindrical counterparts: one is the internal "m = 1" and the other is the external "m = 2" mode. For the equilibria considered here, the external mode is stable with the wall on the plasma, but it becomes unstable for wall radii $b \gtrsim 1.1a$. Figure 3 a shows that, as the aspect ratio is decreased, the "m = 1" mode is stabilized whereas the free boundary "m = 2" mode is only weakly affected by toroidicity. At a certain aspect ratio ($A \approx 3$ for this case) the two branches cross over and the identification of "internal" or "m = 1" and "external" or "m = 2" breaks down. For aspect ratios below the cross over, the branch connected to the large aspect ratio "internal" mode acquires a dominant m = 2 magnetic component and transforms into an "external" mode with a growth rate almost independent of A, while the large aspect ratio "external" branch is stabilized. (The "m = 2" mode is independent of aspect ratio only for low pressure. For higher pressure, the toroidal effects on the "m = 2" mode are stabilizing because of favorable curvature at the q = 2 surface.) Figures 3 b - d show the radial displacement and perturbed magnetic flux for the two different modes at aspect ratio A = 5 and the single unstable mode at A = 2.5. The mixture of m = 1 and m = 2 components with displacements localized around the q = 1 and q = 2 surfaces is evident in all cases, but the phase between the m = 1 and m = 2 components is different for the two branches. For the more unstable branch, the m = 1 and m = 2 magnetic perturbations have the same phase, i.e., reinforce one another on the outboard side.

The cases shown in Fig. 3 indicate that the current profile must be stable to the m = 2/n = 1 tearing mode in the straight tokamak approximation in order to be completely stable at finite aspect ratio and zero pressure. One way to stabilize the m = 2 tearing mode is to decrease q_0 to values substantially below unity. However, for such profiles, the shear must be reduced locally at the q = 1 surface in order for the m = 1 resistive kink to remain stable. Thus, at zero pressure, *free boundary* stability can be achieved at finite aspect ratio by a TEXTOR type profile[4] with q_0 well below unity and low shear at the q = 1 surface induced by shoulders in the current profile. An example of such a profile is shown in Fig. 4. The free boundary growth rates for this equilibrium are shown as functions of aspect ratio in Fig. 5. The *external* mode is now *completely stable* and the internal mode is stabilized for aspect ratios below approximately 10. The shear at q = 1 for this equilibrium is $s \approx 0.035$, which is similar to the low shear profiles in Fig. 2, but the internal mode is stabilized at much larger aspect ratio than for the monotonic I* profile.

The examples in Figs. 3 - 5 show that the stability of the resistive internal kink at zero pressure is sensitive to the current profile, aspect ratio and wall position. Coupling to the external "m = 2" mode becomes important at low aspect ratio. Stability to both internal and external free boundary modes at zero pressure requires non-monotonic current profiles of the TEXTOR type. In the following, we shall often consider the purely internal modes by imposing a fixed boundary.

III. Pressure effects

III. A Theory

A main factor for the stability of the internal kink is pressure. The *global* effects of pressure are described primarily by the poloidal beta at the q = 1 surface.[2] For general cross sections, we use the following definition:

$$\beta_p(\psi) \equiv - \frac{4}{\mu_0 I_\phi^2(\psi) R_m} \int_0^\psi \frac{dp}{d\psi'} V(\psi') \, d\psi' \ , \qquad (4)$$

where $I_\phi(\psi)$ is the toroidal current flowing through a constant-ψ surface, $V(\psi)$ the enclosed volume and R_m is the major radius of the magnetic axis. The poloidal beta at the q = 1 surface will be referred to simply as β_p. The large aspect ratio theory of Bussac et al[2] for circular cross sections predicts an ideal stability limit in β_p. This limit varies considerably with the current profile.[22]

In addition to global effects, pressure also has *local* effects on interchange stability. These are of particular importance for equilibria with low shear at the q = 1 surface. We find that the combination of low shear and ellipticity easily leads to violation of the resistive, and even the ideal, interchange criterion, and that violation of the *ideal* interchange criterion on the q = 1 surface gives rise to a global "m =1" / n = 1 mode with a rather high growth rate.

The ideal[23] and resistive[24] interchange criteria are given by

$$- D_I \equiv \left(\frac{p' T I_2}{q'} - \frac{1}{2}\right)^2 + \frac{p'}{q'^2} (I_5' - p' I_3) (T^2 I_1 + I_4) > 0 \ , \qquad (5a)$$

$$- D_R \equiv - D_I - \left(H - \frac{1}{2}\right)^2 > 0 \ , \qquad (5b)$$

where $T = T(\psi) = RB_\phi$ and

$$H = \frac{Tp'}{q'} \left(I_2 - I_5 \frac{T^2 I_1 + I_4}{T^2 I_4 + I_6}\right) \ , \qquad (5c)$$

$$2\pi \{ I_1, I_2, I_3, I_4, I_5, I_6 \}$$

$$= \int_{\psi = \text{const}} J \, d\chi \left\{ \frac{1}{R^2 |\nabla\psi|^2}, \frac{1}{|\nabla\psi|^2}, \frac{R^2}{|\nabla\psi|^2}, \frac{1}{R^2}, 1, \frac{|\nabla\psi|^2}{R^2} \right\} . \qquad (5d)$$

To discuss the effects of shaping, we give here the simplified expressions obtained from a large aspect ratio expansion. The flux surfaces are assumed to have the form

$$R = R_0 - [r - E(r)] \cos\omega - \Delta(r) + T(r) \cos 2\omega + R_0\, O(\varepsilon^3) \ ,$$

$$Z = \quad [r + E(r)] \sin\omega \quad + T(r) \sin 2\omega + R_0\, O(\varepsilon^3) \ ,$$

where E is the elliptic deformation related to the elongation by $\kappa = 1 + 2E/r + O((E/r)^2)$, $\Delta(r)$ is the Shafranov shift, and T(r) is the triangular deformation related to the triangularity by $\delta = 4T(r)/r$. Keeping the terms proportional to E and T to first order, we obtain from an expansion to second order in ε [where E/r is considered as $O(\varepsilon^0)$ and T/r as $O(\varepsilon^1)$ and μ_0 is set to 1]:

$$-D_I = \frac{1}{4} + \frac{2p'}{rB^2}\frac{q^2}{q'^2}\left[1 - q^2 + \frac{3q^2}{4}\left(\frac{E}{r} + E'\right) + \frac{3q^2}{2}\Lambda\left(\frac{E}{r} - E'\right)\right.$$

$$\left. - \frac{R_0 q^2}{r}\left(\frac{2ET}{r^2} + \frac{6E'T}{r} + \frac{7ET'}{2r} - \frac{3}{2}E'T'\right)\right], \qquad (6a)$$

$$-D_R = \frac{2p'}{rB^2}\frac{q^2}{q'^2}\left\{\left[1 - q^2 + \frac{3q^2}{4}\left(\frac{E}{r} + E'\right) + \frac{3q^2}{2}\Lambda\left(\frac{E}{r} - E'\right)\right.\right.$$

$$\left. - \frac{R_0 q^2}{r}\left(\frac{2ET}{r^2} + \frac{6E'T}{r} + \frac{7ET'}{2r} - \frac{3}{2}E'T'\right)\right]$$

$$\left. + rqq'\left[-\Lambda + \left(\frac{3\Lambda}{2} + \frac{1}{4}\right)E' + \frac{R_0}{r}\left(\frac{ET}{r^2} + \frac{E'T}{r} + \frac{ET'}{r} - \frac{3}{2}E'T'\right)\right]\right\}. \qquad (6b)$$

Here, prime denotes differentiation with respect to the minor radius r and $\Lambda \equiv R_0\Delta'/r$. To the lowest order, this is given by $\Lambda = \beta_p(r) + \ell_i(r)/2$, where $\ell_i(r)$ is the internal inductance. The expressions (6a,b) generalize the formulae for circular flux surfaces of Shafranov and Yurchenko[25] and Glasser, Greene and Johnson.[26] The derivation of (6) will be given elsewhere. Within the large aspect ratio expansion, E(r) and T(r) satisfy second order differential equations with respect to r.

The form (6a) for the Mercier criterion is consistent with previous expressions retaining shaping effects near the magnetic axis[27] [obtained by letting $q' \to 0$ and taking E/r and T/r^2 constant in (6a)]. For the internal kink mode, a useful approximation of (6) is obtained by considering almost flat current profiles with q' small and E/r and T/r^2 constant [taking $s = O(E/r)$ and dropping terms $O((E/r)^2)$] . Together with $q = 1$, this gives

$$-D_I \approx \frac{1}{4} + \frac{rp'}{s^2B^2}\frac{3E}{r}\left(1 - \frac{8T}{r}\frac{R_0}{r}\right) \ , \qquad (7a)$$

$$-D_R \approx \frac{rp'}{s^2B^2}\left[\frac{3E}{r}\left(1-\frac{8T}{r}\frac{R_0}{r}\right)-2s\Lambda\right] \quad , \tag{7b}$$

Equation (7b) shows that if the shear is small (and higher order corrections are negligible) a slight ellipticity, $e \equiv E/r > 2s\Lambda/3$, leads to violation of the resistive interchange criterion. For larger elongations, such as JET shape, even ideal interchange instability can occur for modest pressure and not-so-low shear. As an example, we assume that triangularity is negligible and the pressure profile is parabolic [$\beta_p = -(p'/rB^2)(R^2q^2/2)$]. The Mercier criterion (7a) then reduces to $\beta_p < s^2/(24e\varepsilon^2)$. Even though the expansion to first order in ellipticity is not very accurate for JET geometry, we consider a JET-like case with $\varepsilon_{q=1} = 0.16$ and $e_{q=1} = 0.2$ for which (7a) gives $\beta_p < 8\ s^2$. Evidently, ideal instability may be expected for rather modest pressures when the shear is less than about 0.1. This is confirmed by numerical evaluation of the Mercier criterion without recourse to geometrical orderings.

III.B Numerical results for low shear equilibria with different cross sections

To illustrate the significance of the layer effects for the internal kink mode, we show in Figs. 6 - 8 the resistive growth rates vs. inverse aspect ratio for three different cross sections: circle ($\kappa = 1$, $\delta = 0$) in Fig. 6, slightly oblate ($\kappa = 0.9$, $\delta = 0$) in Fig. 7 and JET shape ($\kappa = 1.7$, $\delta = 0.3$) in Fig. 8. In all these cases, $\beta_p = 0.05$ and $S = 10^7$, and we have used the low-shear current profile of Sec. II, for which $q_0 \approx 0.935$. The pressure profiles are characterized by $dp/d\psi$ = const except for the outer 10 % of the poloidal flux, where pressure gradient goes smoothly to zero at the edge.

Figure 6 a shows the resistive growth rates vs. ε for equilibria with a circular boundary, $\beta_p = 0.05$ and two different wall positions b = a and b = 1.2 a. The behavior at large aspect ratio is similar to the corresponding zero pressure case in Fig. 2. The major effect of finite pressure is that the *fixed boundary* mode remains unstable also at low aspect ratio. This mode is now predominantly "m = 1" and is only weakly dependent on the wall position. It is driven unstable by interchange effects. Figure 6 b shows that the resistive interchange criterion becomes increasingly violated at low aspect ratio. The principal reason for this appears to be the slight "natural" ellipticity of the *internal* flux surfaces that occurs at finite aspect ratio. The ellipticity $e_{q=1}$ of the q = 1 surface is also shown in Fig. 6 b. With a circular boundary, the ellipticity is, to leading order, proportional to ε^2, and for the sequence of equilibria in Fig. 6, a good numerical fit is $e_{q=1} = 5.98 \times 10^{-2}\,\varepsilon^2 + 2.06 \times 10^{-2}\,\varepsilon^4$ (with $\varepsilon \equiv a/R_0$). For $A < 3$, the destabilizing ellipticity correction in the resistive interchange criterion dominates over the shear term. Thus, even though the plasma boundary is circular, the $O(\varepsilon^2)$ modifications of the shape of the internal surfaces change the stability of the internal kink significantly at relevant aspect ratios. This current profile is sensitive to "small" effects because of the low shear on q = 1, but similar behavior is observed for the equilibrium of moderate shear in paragraph II.B. [For the sequence of equilibria in Fig. 6, where the current

profile is held fixed, the shear depends weakly on the aspect ratio, but this is not of primary importance. A good numerical fit is $s = (2.99 + 14.0\ \varepsilon^2 - 9.3\ \varepsilon^4) \times 10^{-2}$. It should be remarked that the large aspect ratio expansion that led to (6) is not strictly valid when the ellipticity is of order ε^2, but (6) nevertheless seems to give a good approximation.]

Figure 7 a shows the growth rate for the case with a weakly oblate boundary ($\kappa = 0.9$). As the aspect ratio decreases, these equilibria first become overstable and are then stabilized. The resistive interchange criterion is satisfied, see Fig. 7 b. In this respect, the important difference from the case of a circular boundary is that the $q = 1$ surface remains oblate also for small aspect ratios [the ellipticity is well fitted numerically by $E/r = (-4.09 + 6.6\ \varepsilon^2) \times 10^{-2}$]. For these equilibria with a slightly oblate boundary and moderate pressure, the internal kink mode is completely stable at low aspect ratio. Although the favorable curvature is important for completely stabilizing the mode, the stabilization at small aspect ratio is mainly a global (Δ') effect similar to the zero beta case. Note that even though both the deviation from circular boundary ($\kappa = 0.9$) and the S-number (10^7) are modest, the resistive internal mode behaves quite differently than in the case of a circular boundary. With more pronounced shaping and larger S the influence of curvature of course becomes stronger.

Figure 8 a shows the growth rates for the JET-shaped equilibrium ($\kappa = 1.7$, $\delta = 0.3$). These results differ clearly from those of the two previous cases. With JET shape and $\beta_p = 0.05$, the growth rate *increases* with ε for $\varepsilon \geq 0.08$. The internal kink is now *ideally* unstable for $\varepsilon > 0.21$ and its growth rate is high ($> 5 \times 10^{-3}\ \omega_A$) at low aspect ratio. The reason for the ideal instability at low β_p can be seen in Fig. 8 b: the ideal interchange criterion is violated for $\varepsilon > 0.22$. Thus, ideal instability sets in almost exactly when (actually slightly before) the Mercier criterion is violated and the growth rate soon reaches rather high values. For $0.14 < \varepsilon < 0.22$, the resistive, but not the ideal, interchange criterion is violated and the equilibrium is resistively unstable with much smaller growth rates.

It may be noted, as a curiosity, that for large aspect ratios, $\varepsilon < 0.14$, the resistive interchange criterion is satisfied for these JET-shaped equilibria and the growth rate at moderate pressure is reduced *below* the zero beta value. This is connected to the stabilizing influence of triangularity in combination with ellipticity, readily seen in Eq. (7). For fixed shape (E, T independent of ε) the stabilizing terms proportional to $E \times T$ become dominant at large aspect ratio. Of course in the limit of $\varepsilon \to 0$ with β_p fixed, the pressure effects become negligible ($D_I \to -1/4$ and $D_R \to 0$), and the straight tokamak internal kink mode reappears. This is shown by Fig. 8 a where the growth rate increases again for $\varepsilon < 0.05$.

IV. Current profile effects

IV. A Circular shape

In this section, we study the influence of the current profile in combination with finite pressure and shaping and discuss how the triggering of a sawtooth crash might be related to changes in the current profile. We first consider circular cross section and the two types of current profiles used in Sec. II, the centrally flat current profile (I) and the TEXTOR profile (II). To generate families of self-similar profiles, we apply a uniform scaling of the toroidal current density, keeping the poloidal beta, the internal inductance and the vacuum toroidal field fixed (see Ref. 20 for details). The scaling approximately corresponds to multiplying the q-profile by a certain factor and allows to prescribe the q-value at a specified radius, $q_p = q(\rho_p)$ or the q = 1 radius.

For the centrally flat profile (I), the shear is low in a central region and has a local minimum at $\rho = \rho_p = 0.44$ where $dI^*/d\rho = 0$. Outside this radius, the shear increases rapidly. The local minimum $s(\rho_p)$ is about 0.03 and the central safety factor q_0 is related to q_p by $q_0 \approx 0.935\ q_p$. For $q_p > 1$, the shear at q = 1 is low, but when q_p is decreased below unity, the q = 1 surface moves out into the region of rapidly increasing shear. For $q_p = 1$, the q = 1 surface is located at the radius of minimum shear. Such a set of profiles may correspond approximately to the evolution in time during the ramp phase of a sawtooth, if the preceding crash leads to complete reconnection and almost flat central q, followed by peaking of the current due to trapped particle effects on the resistivity, as suggested in Ref. 28. The same pressure profile $p(\psi)/p_0$ is applied as in Sec. III.B. The central beta is related to β_p (poloidal beta at q = 1) by $\beta_0 \approx 0.096\ \beta_p$ and the volume averaged beta ($\langle\beta\rangle \equiv 2\mu_0\langle p\rangle/\langle B^2\rangle$) by $\langle\beta\rangle \approx 0.039\ \beta_p$. The poloidal beta at the edge is $\beta_p(\rho = 1) \approx 2.73\ \beta_p(q = 1)$.

Figures 9 and 10 show the growth rates of the internal kink mode for the *centrally flat* current profile as functions of q_p at different values of β_p and Lundquist numbers S (6×10^6 in Fig. 9 and 6×10^8 in Fig. 10). In these cases, the aspect ratio is 4 and a conducting wall is assumed at r = b = 1.2a. We note that *complete* resistive MHD stability is never achieved for this profile. However, for $\beta_p \leq 0.05$, the resistive growth-rate is small when the q = 1 surface is in the region of small shear, and the instability is a free boundary mode with a large m = 2 magnetic perturbation, as discussed in Sec. II. Modes with such small resistive MHD growth rates may be stabilized by effects not included in the linear resistive-MHD model.

By comparing Figs. 9 and 10, one can identify regions of resistive and ideal instability. The instabilities for $\beta_p \geq 0.15$ and $q_p < 1$ (i.e., when the q = 1 surface is in the outer region of high shear) are ideal. The normalized growth rates are several times 10^{-3} and are almost independent of the resistivity. The growth rate peaks when the shear at q = 1 is small, as expected for ideal modes.[2,18] For $\beta_p \leq 0.05$, the instabilities are resistive. The growth rates follow the tearing scaling with respect to resistivity and have a minimum when the shear is small at q = 1. (The growth rates are mainly affected by global effects on δW, but the different dependencies of ideal and resistive growth rates on

the local shear can nevertheless be observed in Figs. 9 and 10.) The case $\beta_p = 0.10$ is near marginal stability for an ideal mode when $q_p < 1$ and the instability shows a weaker dependence on S. Figure 10 shows that the resistive growth rates are very small at high S. These growth rates do not even come close to those observed experimentally in sawtooth precursors where, typically, $\gamma/\omega_A > 10^{-3}$.

An interesting feature is evident for the cases with $\beta_p \geq 0.15$ (and also $\beta_p = 0.10$ at high S). The pressure driven instabilities are sensitive to the value of q_p, or to the location of the q = 1 surface with respect to the "knee" of the q-profile. The finite-beta growth rates have maxima when the q = 1 surface is at the point of minimum shear and remain high when the q = 1 surface reaches the outer, high-shear region. Thus, depending on the evolution in time of the experimental profiles, a "pressure driven" instability may be triggered by changes in the current profile rather than by an increase in the pressure itself. If we invoke stabilization of a weak resistive-MHD instability by some unspecified mechanism, a sawtooth crash could be triggered by the increase in MHD growth rates when the q = 1 surface approaches, or moves out into, the outer high-shear region. Such a trigger mechanism for the sawteeth may explain why the inversion radius remains almost constant between successive crashes. A "knee" in the q-profile created by reconnection during the preceding crash would only be partially smoothed out by resistive diffusion before the next crash and could then act as a *spatially localized magnetic trigger* for the following sawtooth.

For comparison with other geometries, we note that the resistive interchange criterion generally indicates stability for circular cross section with A = 4, but D_R takes small numerical values (due to finite shear rather than favorable curvature). It may be noted that the growth rates are generally slightly higher for $\beta_p = 0$ than for $\beta_p = 0.05$ which is explained by the increased inertia associated with the motion along the field lines in the finite beta case.

The details of the results in Figs. 9 and 10 depend on the choice of the current profile. For instance, if the central shear is reduced, the ideal pressure driven instabilities are enhanced, while the growth rates of the resistive instabilities for low pressure are reduced. The inverse holds for profiles with larger central shear.

Next, we consider current profile of the TEXTOR type. The shoulders in I* have been adjusted so that the shear has a minimum of about 0.034 at $\rho = \rho_p \approx 0.44$, the central q is $q_0 \approx 0.634\ q_p$ and the aspect ratio is 4. Figures 11 and 12 show the growth rates for different S and $\beta_p = 0.0$, 0.1, 0.2, and 0.3. The behavior is similar to that for the centrally flat profiles, but the TEXTOR profile supports about twice the pressure before becoming ideally unstable and the growth rates are very sensitive to the q = 1 location at high pressure, $\beta_p \geq 0.2$. For the TEXTOR profile, there is indeed an interval in q_p where the equilibrium is *entirely* stable. However, this interval is small, and certainly less than the shift in q during the sawtooth cycle. This again indicates that the resistive kink mode is stabilized during most of the sawtooth cycle by effects not included in the linear resistive MHD model.

As discussed in Sec. II, low aspect ratio is stabilizing for the internal kink mode. An example is given by Fig. 13 which shows the growth rate γ as a function of q_p for a

sequence of equilibria with aspect ratio A = 2.5 and TEXTOR profiles. Figure 13 refers to an S-number of 6×10^8 and differs from Fig. 12 only with respect to the aspect ratio. We note that the region of complete stability is larger at the smaller aspect ratio and that there is even a small interval in q_p giving complete resistive stability for $\beta_p = 0.20$.

IV. B JET shape

As noted in Sec II, the large elliptic deformation of the q = 1 surface in a JET-shaped cross section ($\kappa = 1.7$, $\delta = 0.3$, A = 2.7) can lead to ideal instability at moderate pressure if the shear at q = 1 is small. Therefore, we consider current profiles with higher shear in this section. To show the dependence on the shear, we choose two values of the minimum shear for each of the two types of profiles: "centrally flat" denoted (I-H) and (I-L) for high and low shear respectively, and "TEXTOR" denoted (II-H) and (II-L). The shear at q=1 is shown in Fig. 14 for the four profiles vs $q_p = q(\rho=\rho_p \approx 0.41)$. The fixed boundary growth rates for $S = 6 \times 10^8$ are shown for $\beta_p = 0$ in Fig. 15, for $\beta_p = 0.05$ in Fig. 16 and for $\beta_p = 0.10$ in Fig. 17.

Figure 15 shows that there are only minor differences between the growth rates for the four current profiles at zero pressure. These growth rates are generally lower than in the circular case at A = 4. However, the JET cross section is more sensitive to pressure, and a clear increase in growth rates resulting from $\beta_p = 0.05$ is evident in Fig. 16. Notably, there is no case that is completely stable for this pressure. However, the large shear profiles have low growth rates for $\beta_p = 0.05$, in particular with the TEXTOR current profile. The pressure driven instability for the low shear TEXTOR profile is highly sensitive to the q-value.

For higher pressure, $\beta_p = 0.10$ (see Fig. 17), the two centrally flat profiles both give rather high growth rates for all values of q_p, whereas the TEXTOR profile gives normalized growth rates as low as a few times 10^{-4} when $q_p > 1$, i.e., when the q = 1 surface is inside the "shoulder".

IV. C Oblate cross section

To illustrate the importance of the average curvature, we again consider the slightly academic example of an oblate cross section. We choose a plasma boundary given by (1) with $\kappa = 0.9$, $\delta = 0$ and the aspect ratio is A = 4. The current profile is of the TEXTOR type with a minimum shear of 0.042. The result for $\beta_p = 0.05$ and $S = 6 \times 10^7$ is shown in Fig. 18. When the q = 1 surface is located near the radius of minimum shear, the growth rate becomes complex, and in a certain interval, $0.995 \lesssim q_p \lesssim 1.005$, the mode is stabilized. The complex frequency shows that the mode is stabilized by favorable average curvature. The resistive interchange parameter - D_R reaches a maximum of about 0.07 for $q_p = 1$.

For higher pressure, $\beta_p = 0.10$, and oblate cross section, the destabilizing global effects of pressure dominate over the stabilizing layer effects, and the resistive internal kink is no longer stable for any $q_0 < 1$.

V. Summary and discussion

The internal kink mode is sensitive to a large number of effects, and the following summary is an attempt to delineate the most important of these.

For *zero pressure*, the resistive MHD stability of the internal kink is influenced primarily by the aspect ratio and the current profile $I^* = \langle j_\phi/R \rangle / \langle 1/R \rangle$. Low aspect ratio is stabilizing. Stability is improved by low shear at the $q = 1$ surface but also by low q_0. Equilibria with monotonic I^* are stable with a fixed boundary when the aspect ratio is below a threshold value that varies inversely with the shear. Free boundary stability appears to require non-monotonic I^*. Current profiles of the TEXTOR type[4] with shoulders near the $q = 1$ surface are much more stable than monotonic profiles and can remain completely stable with a free boundary at very large aspect ratios.

The internal kink stability is affected by shaping already at zero pressure. The shaping effects are more pronounced at large aspect ratio where the toroidal stabilization is weak. Ellipticity alone is destabilizing, but a combination of ellipticity and sufficient triangularity, such as JET shape, is more stable than a circular equilibrium.

Central pressure gradients are generally strongly destabilizing for the resistive internal kink mode. Part of the reason for this is global (i.e., Δ') effects on the eigenfunction. However, local *interchange* effects at the $q = 1$ resonant surface are important, in particular when the shear is low, and this makes the stability at finite pressure highly sensitive to shaping. For many shapes of interest, notably, JET shape, the curvature at the $q = 1$ surface is unfavorable because of ellipticity, and the resistive interchange criterion is violated for low shear (and finite pressure). For JET-shaped cross section, we do not find any profile that is resistively stable with $q_0 < 1$ and poloidal beta at the $q = 1$ surface of order 0.05. At low shear, even the Mercier criterion can be violated at pressures well below the Bussac limit.[29] This typically leads to global ideal internal kinks with rather high growth rates. A more detailed study of the ideal stability will be presented elsewhere.

The sensitivity of the resistive MHD stability to the layer effects and geometry was exemplified by the observation that for equilibria with a *circular* boundary, even the slight natural ellipticity of the $q = 1$ surface at low aspect ratio can destabilize a resistive interchange driven internal kink if the shear is low. For an oblate boundary, where the curvature at $q = 1$ is favorable also at low aspect ratio, the layer effects are stabilizing, and a finite window of free boundary stability exists for moderate β_p.

One conclusion of the present study is that despite the stabilizing effects of low aspect ratio on the internal kink mode, *complete* resistive MHD stability is difficult to achieve when finite pressure and free boundary are taken into account. It appears unlikely that such stringent stability conditions can be met during the entire ramp phase of the sawtooth cycle when the internal kink mode is manifestly stable. When confronted with the experimental observations of $q_0 < 1$, this leads us to conclude that the criterion of complete resistive MHD stability is too stringent and that weak resistive instabilities are stabilized by effects not included in the linear MHD model.

Nevertheless, finite aspect ratio effects are strongly stabilizing and often reduce the resistive kink mode to a weak tearing/resistive interchange instability with a growth rate that becomes very small at high S. In particular, the growth rate is often well below $10^{-3}\ \omega_A$, which is a characteristic growth rate of sawtooth precursors, e.g., in JET. If we adopt $10^{-3}\ \omega_A$, or a value of the order of the diamagnetic frequency as an *ad hoc* threshold for stability, the stability boundary in large tokamaks will be close to the ideal stability boundary. (For such modes one may expect important effects of electron inertia.[30-32])

Several effects are known which can stabilize weak resistive-MHD instabilities. One is nonlinear saturation of tearing/resistive interchange modes at finite island size. A finite island reduces the destabilizing layer effects that are dominant at small resistivity for elliptic shaping. Nonlinear saturation by the reduced destabilization from unfavorable curvature is the inverse process to the nonlinear destabilization of tearing modes by finite island size in regions of favorable curvature discussed by Kotschenreuther et al.[33] In addition, the effective layer width may increase, and therefore the effect of curvature decrease, as a consequence of microturbulence. We mention that nonlinear simulations[34] of the sawtooth activity based on the "straight tokamak" resistive MHD model showed generally good agreement with experimental results for low Lundquist numbers ($S < 10^7$), while difficulties appeared for higher values of S, where more detailed physics effects should be important.

Other mechanisms for stabilizing modes that are weakly unstable in resistive MHD are offered by more detailed physics models, including diamagnetic rotation[3,15,16] and trapped particle effects.[11,12,17] It appears clear that non-MHD effects, and/or nonlinearity, have to be taken into account in order to understand the behavior of the sawteeth in large tokamaks, in particular, for auxiliary heating experiments. The present study has nevertheless shown a number of parametric dependencies, and points out the importance of the curvature effects at the $q = 1$ surface. If the stability of the internal kink mode is governed by linear theory, curvature effects should be significant also when more detailed physics models are applied.

References

1. B.B. Kadomtsev, Sov. J. Plasma Phys. **1**, 389 (1975) [Fiz. Plasmy **1**, 710 (1975)].
2. M.N. Bussac, R. Pellat, D. Edery, and J. Soulé, Phys. Rev. Lett. **35**, 1638 (1975).
3. M.N. Bussac, R. Pellat, D. Edery, and J. Soulé, in *Plasma Physics and Controlled Nuclear Fusion Research 1976*, Proceedings of the 6th International Conference, Berchtesgaden (IAEA, Vienna, 1977), Vol. 1, p. 607.
4. H. Soltwish, W. Stodiek, J. Manickam, and J. Schlüter, in *Plasma Physics and Controlled Nuclear Fusion Research 1986*, Proceedings of the 11th International Conference, Kyoto (IAEA, Vienna, 1987), Vol. 1, p. 263.
5. J. O'Rourke, J. Blum, J.G. Cordey, A. Edwards, N. Gottardi, B. Keegan, E. Lazzaro, G. Magyar, Y. Stephan, P. Stubberfield, D. Véron, and D. Zasche, in *Controlled Fusion and Plasma Heating*, Proceedings of the 15th European Conference, Dubrovnik, 1988, (European Phys. Soc., Geneva, 1988) Vol 12B, Part I, p. 155.
6. A. Weller, A.D. Cheatham, A.W. Edwards, R.D. Gill, A. Gondhalekar, R.S. Granetz, J. Snipes, and J.A. Wesson, Phys. Rev. Lett., **59**, 2303 (1987).
7. H. Soltwish, private communication (1990).
8. H. Weisen, G. Borg, B. Joye, A.J. Knight, and J.B. Lister, Phys. Rev. Lett. **62**, 434 (1989).
9. K. McCormick, A. Eberhagen, H. Murmann and the ASDEX Team, in *Controlled Fusion and Plasma Heating*, Proceedings of the 15th European Conference, Dubrovnik, 1988, (European Phys. Soc., Geneva, 1988) Vol 12B, Part I, p. 35.
10. J.A. Holmes, B.A. Carreras, and L.A. Charlton, Phys. Fluids **B1**, 788 (1989).
11. R.B. White, P.H. Rutherford, P. Colestock, and M.N. Bussac, Phys. Rev. Lett. **60**, 2038 (1988); R.B. White, M.N. Bussac, and F. Romanelli, Phys. Rev. Lett. **62**, 539 (1989).
12. F. Porcelli, Plasma Phys. Controlled Fusion **33**, 1601 (1991).
13. K. Hanada, H. Tanaka, M. Iida, S. Ide, T. Minami, M. Nakamura, T. Maekawa, Y. Terumichi, S. Tanaka, M., Yamada, J. Manickam, and R.B. White, Phys. Rev. Lett. **66**, 1974 (1991).
14. D.J. Campbell, D.F.H. Start, J.A. Wesson, et al, Phys. Rev. Lett. **60**, 2148 (1988).
15. G. Ara, B. Basu, B. Coppi, G. Laval, M.N. Rosenbluth, and B.V. Waddell, Ann. Phys. **112**, 443 (1978).
16. J.F. Drake, T.M. Antonsen Jr., A.B. Hassam, and N.T. Gladd, Phys. Fluids **26**, 2509 (1983).
17. J.W. Connor and R.J. Hastie, Phys. Fluids **19**, 1727 (1976); T.M. Antonsen, Jr., B. Lane, and J.J. Ramos, Phys. Fluids **24**, 1465 (1981).
18. R.J. Hastie, T.C. Hender, B.A. Carreras, L.A. Charlton, and J.A. Holmes, Phys. Fluids **30**, 1756 (1987).

19. G. Vlad, H. Lütjens, and A. Bondeson, in *Controlled Fusion and Plasma Heating*, Proceedings of the 18th European Conference, Berlin, 1991, (European Phys. Soc., Geneva, 1991), Vol 15C, Part IV, p. 85.
20. H. Lütjens, A. Bondeson, and A. Roy, Comput. Phys. Comm. (in press).
21. D. Edery, G. Laval, R. Pellat, and J.L. Soulé, Phys. Fluids **19**, 260 (1976).
22. A. Bondeson and M.-N. Bussac, "Stability of the n =1 ideal internal kink mode for large aspect ratio Shafranov equilibria", to be published in Nucl. Fusion (1992).
23. C. Mercier, Nucl. Fusion **1**, 47 (1960).
24. A.H. Glasser, J.M. Greene, and J.L. Johnson, Phys. Fluids **18**, 875 (1975).
25. V.D. Shafranov and E.I. Yurchenko, Sov. Phys. JETP **26**, 682 (1968).
26. A.H. Glasser, J.M. Greene, and J.L. Johnson, Phys. Fluids **19**, 567 (1976).
27. J.P. Freidberg, *Ideal Magnetohydrodynamics*, Chap. 10 (Plenum Press, New York, 1987), and references therein.
28. W. Park and D.A. Monticello, Nucl. Fusion **30**, 2413 (1990).
29. B.N. Kuvshinov, Sov. J. Plasma Phys. **17**, 79 (1991) [Fiz. Plasmy **17**, 139 (1991)].
30. J.A. Wesson, Nucl. Fusion **30**, 2545 (1990).
31. F. Porcelli, Phys. Rev. Lett. **66**, 425 (1991).
32. J.F. Drake and R.G. Kleva, Phys. Rev. Lett. **66**, 1458 (1991).
33. M. Kotschenreuther, R.D. Hazeltine, and P.J. Morrison, Phys. Fluids **28**, 294 (1985).
34. G. Vlad and A. Bondeson, Nucl. Fusion **29**, 1139 (1989).

Figure Captions

FIG. 1 Profiles of (a) surface averaged current density I*, (b) safety factor q, and (c) shear s vs. normalized minor radius $\rho = (V(\psi)/V_{tot})^{1/2}$ for "low-shear" equilibrium.

FIG. 2 Fixed boundary resistive growth rates γ vs. inverse aspect ratio ε, for zero pressure equilibria with different shapes: circle, ellipse (indicated by squares) and JET shape (indicated by triangles) and different central shear (low shear indicated by filled symbols, high shear by open symbols). The S-number is 10^6.

FIG. 3 a Resistive growth rates γ for $S = 10^6$ vs. inverse aspect ratio ε for a circular equilibrium with low central shear and zero pressure. The filled-in circles refer to the fixed boundary "internal" mode, while the open symbols show the result with a free boundary and a conducting wall at b = 1.2 a.

FIG. 3 b - d Fourier components of radial perturbed velocity $v = \mathbf{v} \cdot \nabla(\psi/\psi_{surf})^{1/2}$ and magnetic flux $b = J\,\mathbf{b} \cdot \nabla(\psi/\psi_{surf})^{1/2}$ [in straight field line coordinates with PEST-1 Jacobian $J = C(\psi)\,R^2$] for the free-boundary modes in (a). (b) "m = 1" mode for A = 5, (c) "m = 2" mode for A = 5, and (d) single unstable mode for A = 2.5. Note that the m = 1 and m = 2 components of the magnetic flux are in phase (reinforce one another on the outboard side) for the fast growing branch (b and d) and out of phase for the slower branch (c).

FIG. 4 Profiles of (a) surface averaged current density I*, (b) safety factor q, and (c) shear s vs. normalized minor radius $\rho = (V(\psi)/V_{tot})^{1/2}$ for "TEXTOR" equilibrium.

FIG. 5 Free boundary resistive growth rates γ for $S = 10^6$ vs. inverse aspect ratio ε for a circular equilibrium with TEXTOR current profile and zero pressure. A conducting wall is assumed at b = 1.2 a. Note the absence of an "m = 2" branch at large aspect ratio and the complete stabilization at low aspect ratio.

FIG. 6 a Resistive growth rates γ for $S = 10^7$ vs. inverse aspect ratio ε for a circular equilibrium with low central shear and $\beta_p = 0.05$. The filled-in circles refer to a fixed boundary, while the open circles show the result with a free boundary and a conducting wall at b = 1.2 a.

FIG. 6 b The resistive interchange parameter - D_R (filled circles) and ellipticity e (open) at the q = 1 surface for the low-shear circular equilibrium.

FIG. 7 a Free boundary growth rates γ for $S = 10^7$ vs. inverse aspect ratio ε for a weakly oblate equilibrium with low central shear and $\beta_p = 0.05$.A conducting wall is assumed at at b = 1.2 a. The open circles show the growth rate and the filled circles the real part of the frequency.

FIG. 7 b The resistive interchange parameter - D_R (filled circles), ellipticity e (open circles), and shear s (open triangles) at the q = 1 surface for the low-shear oblate equilibrium.

FIG. 8 a Fixed boundary growth rates vs. inverse aspect ratio ε for a JET shaped equilibrium with low central shear and $\beta_p = 0.05$. The open circles show the resistive mode for $S = 10^7$ and the filled circles refer to the ideal case.

FIG. 8 b The resistive and ideal interchange parameters - D_R (open circles), and - D_I (filled circles) vs. inverse aspect ratio for the JET shaped low-shear equilibrium.

FIG. 9 Free boundary growth rates for $S = 6 \times 10^6$ vs. q_p (safety factor at the point of minimum shear, $\rho \approx 0.44$) for a circular low-shear equilibrium and different values of β_p (see symbol table). The aspect ratio is 4 and the conducting wall is at b = 1.2 a.

FIG. 10 Free boundary growth rates vs. q_p. All parameters are identical to Fig. 9 except $S = 6 \times 10^8$.

FIG. 11 Free boundary growth rates for $S = 6 \times 10^6$ vs. q_p (safety factor at the point of minimum shear, $\rho \approx 0.44$) for a circular equilibrium with TEXTOR current profile and different values of β_p (see symbol table). The aspect ratio is 4 and the conducting wall is at b = 1.2 a.

FIG. 12 Free boundary growth rates vs. q_p. All parameters are identical to Fig. 11 except $S = 6 \times 10^8$.

FIG. 13 Free boundary growth rates vs. q_p for TEXTOR equilibrium All parameters are identical to Fig. 12 except the aspect ratio A = 2.5. (a) with full range of γ, and (b) on a blown-up scale to show stable region.

FIG. 14 Shear at the q = 1 surface vs. q_p (safety factor at the point of minimum shear, $\rho \approx 0.41$) for JET-shaped equilibria with A = 2.7 and different current profiles. Circles indicate "centrally flat" current, triangles: "TEXTOR"; open symbols: "low shear" and filled symbols: "high shear".

FIG. 15 a Fixed boundary growth rates for $S = 6 \times 10^8$ vs. q_p (safety factor at the point of minimum shear, $\rho \approx 0.41$) for a JET-shaped equilibrium with centrally flat current profile and zero pressure (Fig. 14). Open circles refer to the low-shear and filled circles to the high-shear profile.

FIG. 15 b Fixed boundary growth rates for $S = 6 \times 10^8$ vs. q_p (safety factor at the point of minimum shear, $\rho \approx 0.41$) for a JET-shaped equilibrium with TEXTOR current profile and zero pressure (Fig. 14). Open circles refer to the low-shear and filled circles to the high-shear profile.

FIG. 16 a Identical to Fig. 15 a except $\beta_p = 0.05$. Open circles refer to the low-shear and filled circles to the high-shear profile.

FIG. 16 b Identical to Fig. 15 b except $\beta_p = 0.05$. Open circles refer to the low-shear and filled circles to the high-shear profile.

FIG. 17 a Identical to Fig. 15 a except $\beta_p = 0.10$. Open circles refer to the low-shear and filled circles to the high-shear profile.

FIG. 17 b Identical to Fig. 15 b except $\beta_p = 0.10$. Open circles refer to the low-shear and filled circles to the high-shear profile.

FIG. 18 Free boundary growth rates for $S = 6 \times 10^7$ vs. q_p (safety factor at the point of minimum shear, $\rho \approx 0.44$) for a weakly oblate equilibrium with TEXTOR current profile and $\beta_p = 0.05$. The aspect ratio is 4 and the conducting wall is at b = 1.2 a. Filled circles show the growth rate and open circles the real frequency.

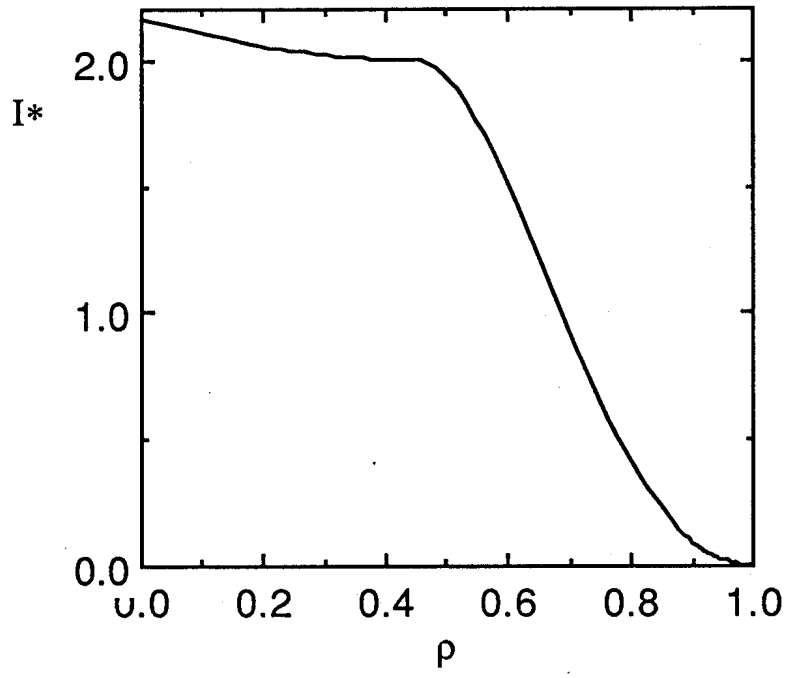

Figure 1 a

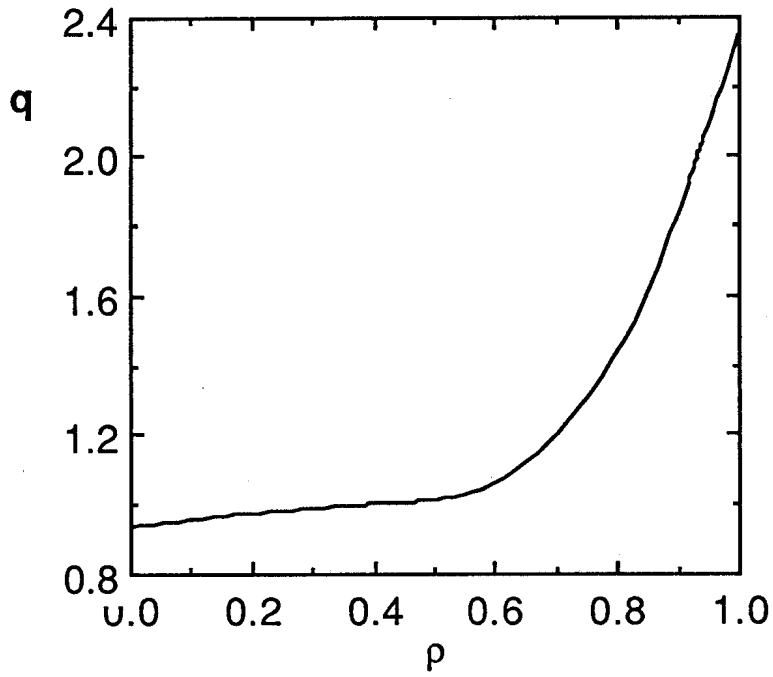

Figure 1 b

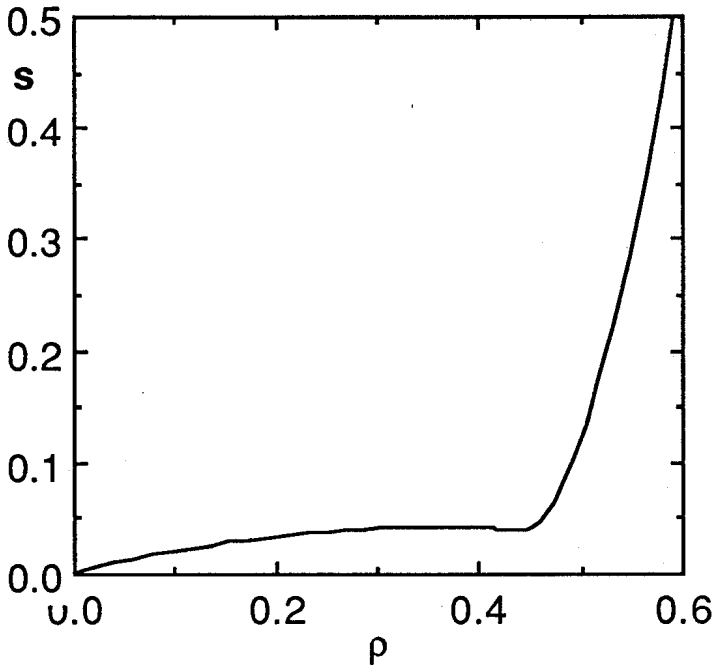

Figure 1 c

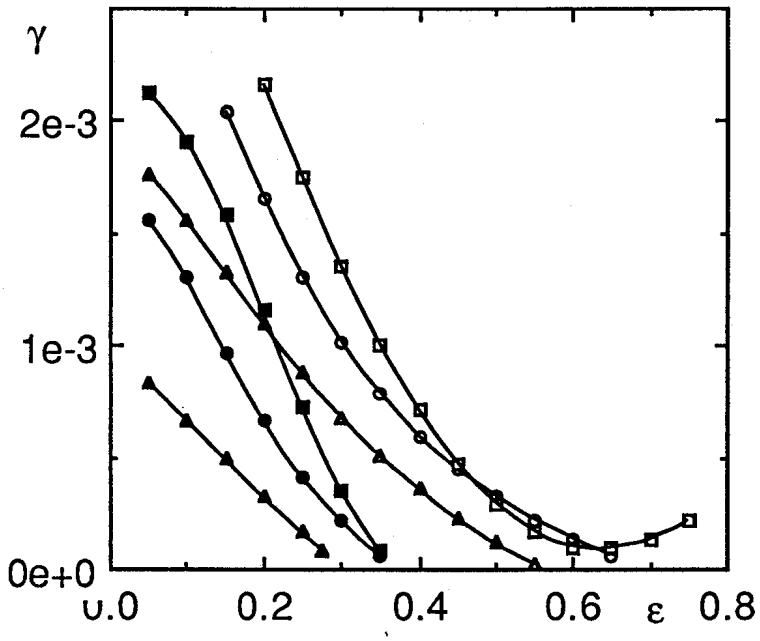

Figure 2

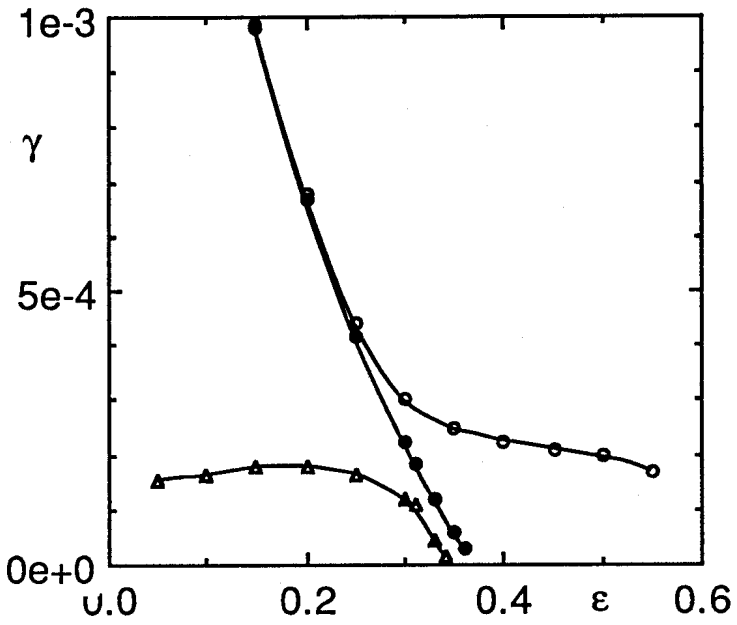

Figure 3 a

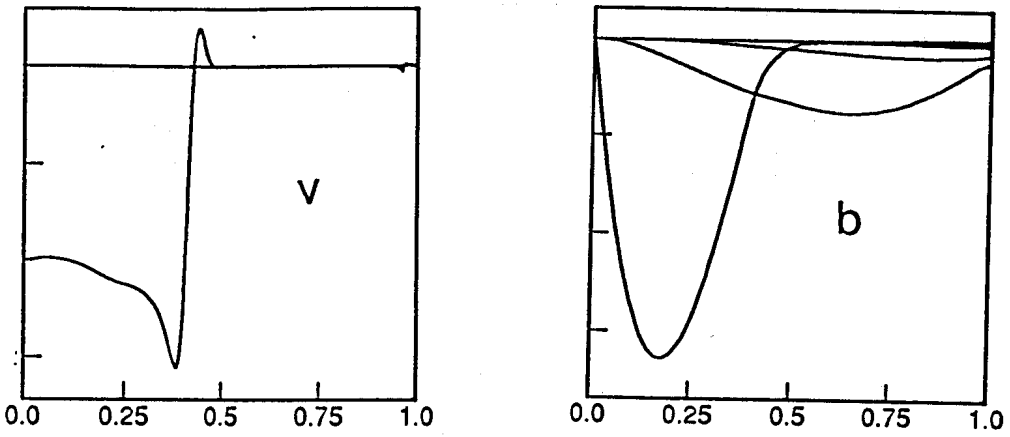

Figure 3 b

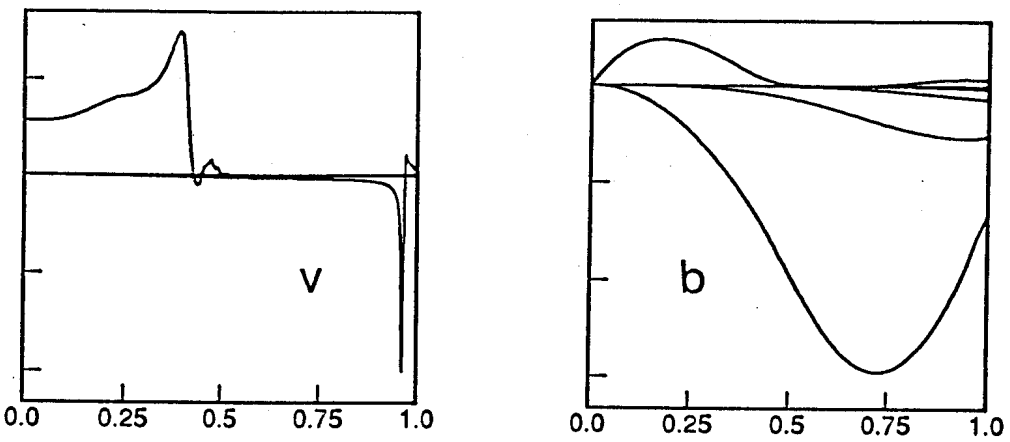

Figure 3 c

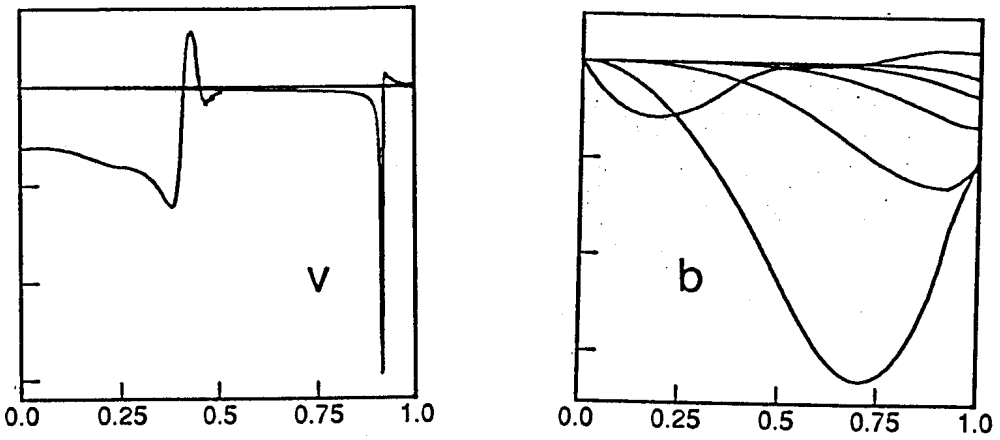

Figure 3 d

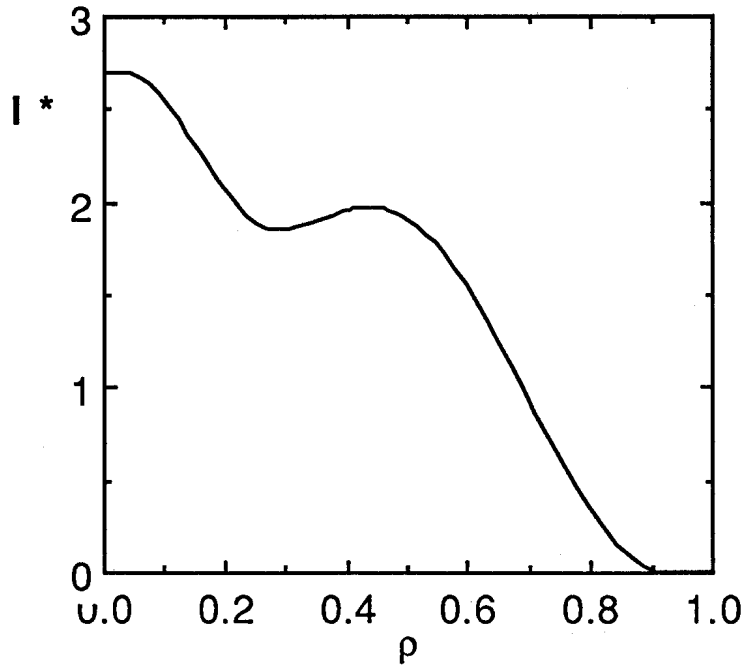

Figure 4 a

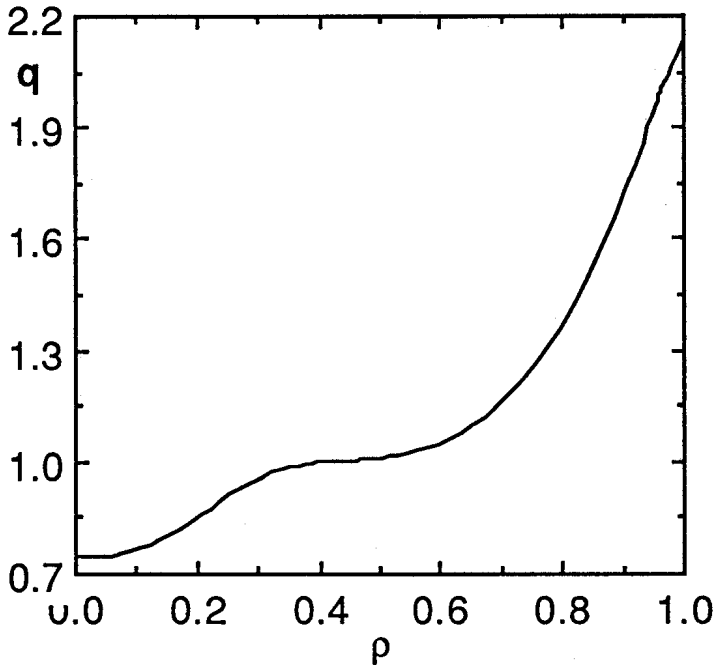

Figure 4 b

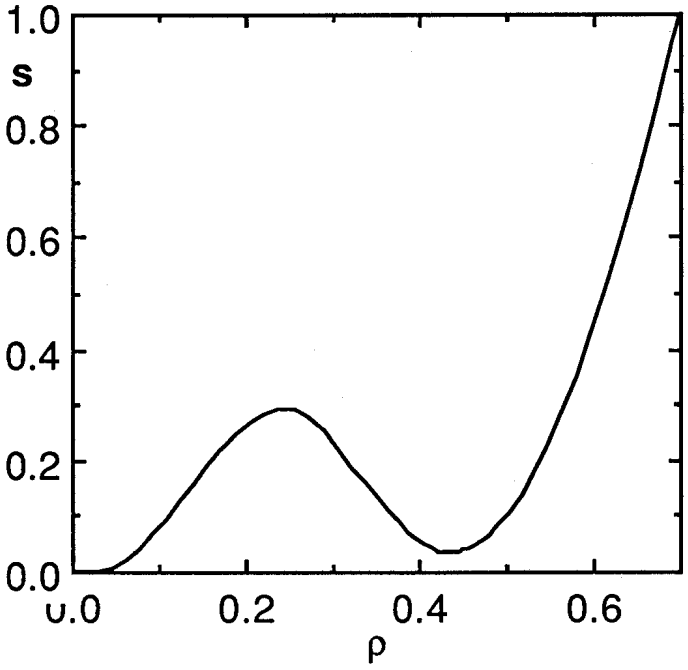

Figure 4 c

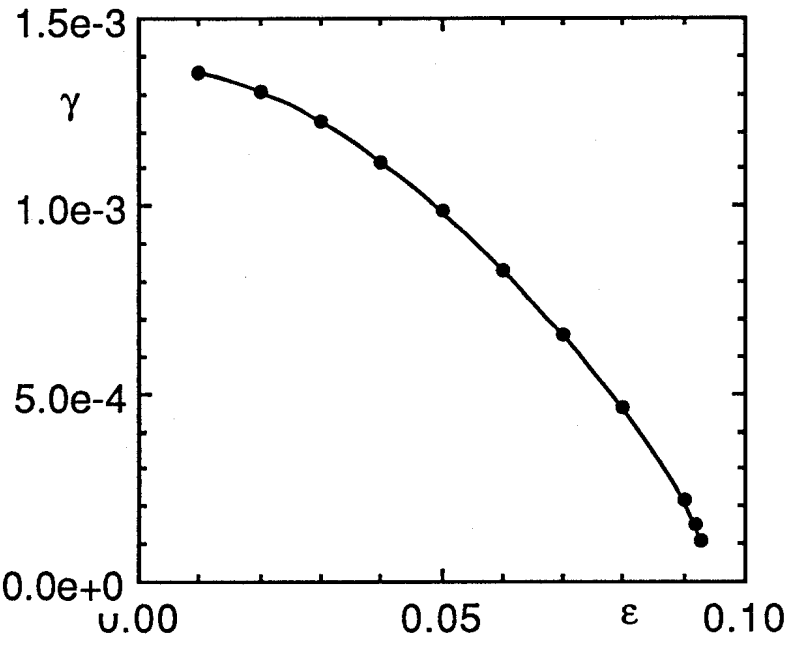

Figure 5

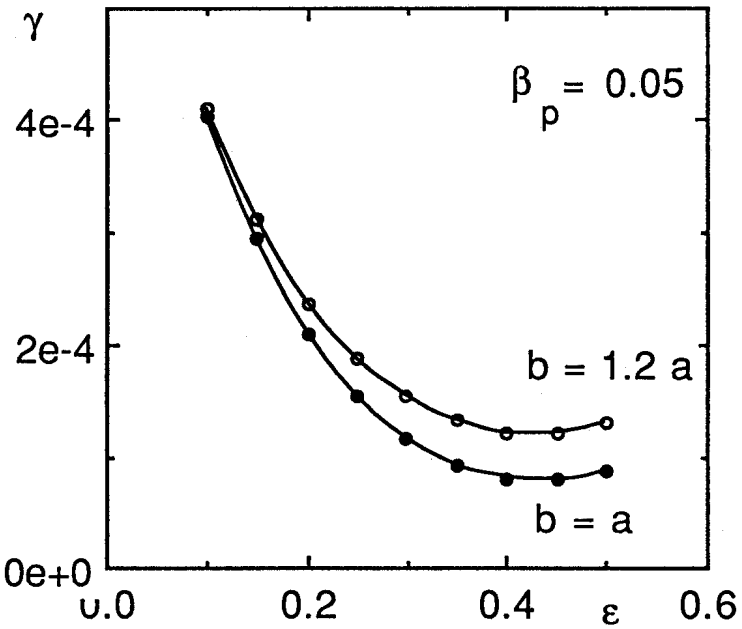

Figure 6 a

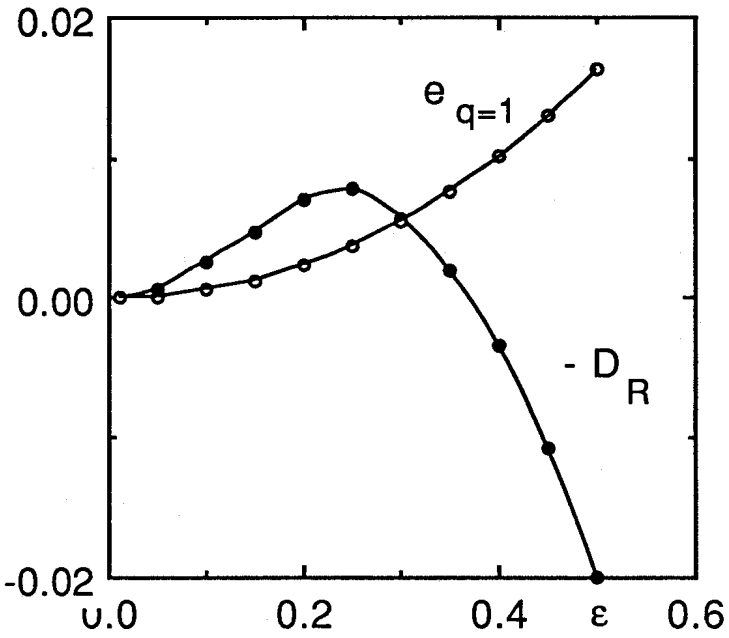

Figure 6 b

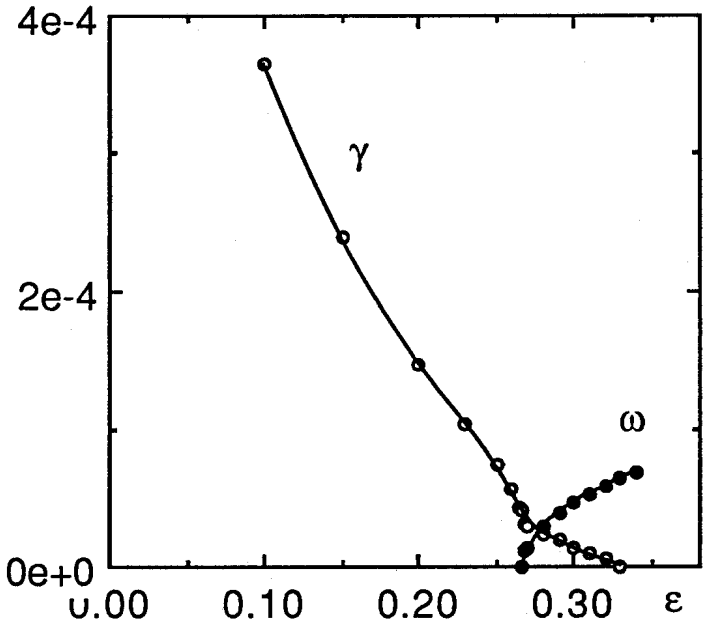

Figure 7 a

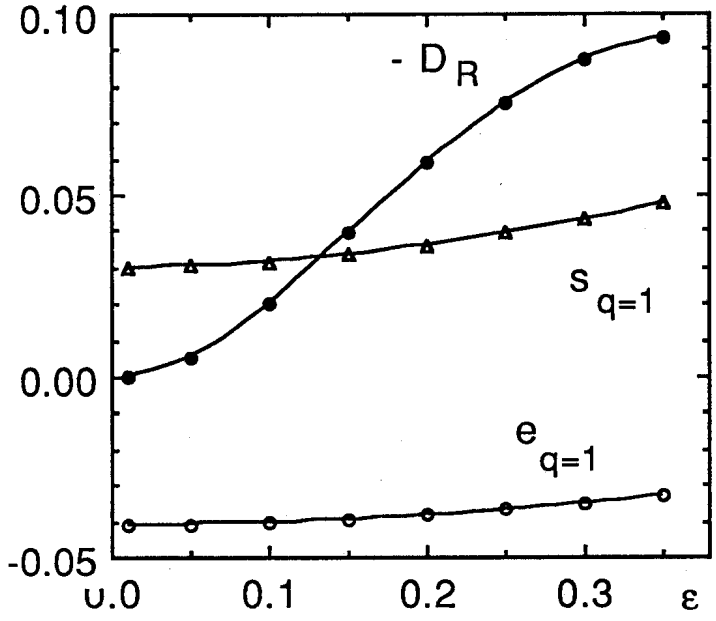

Figure 7 b

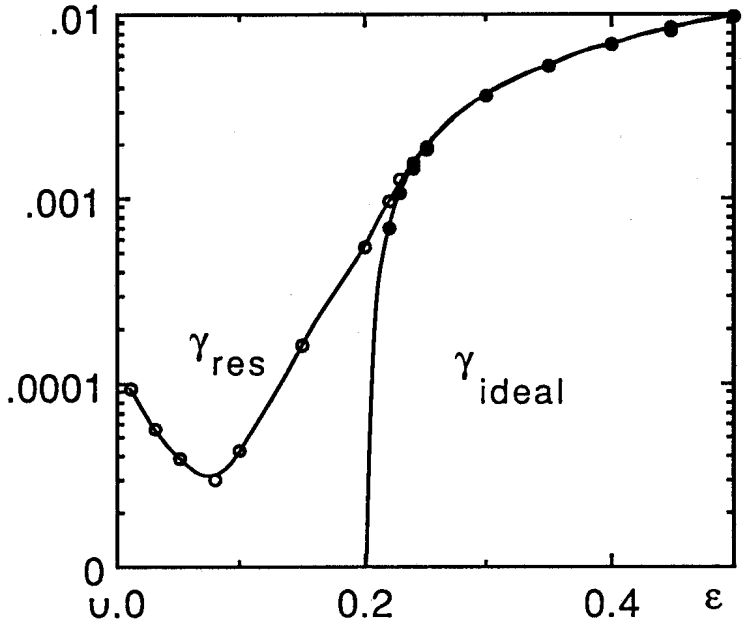

Figure 8 a

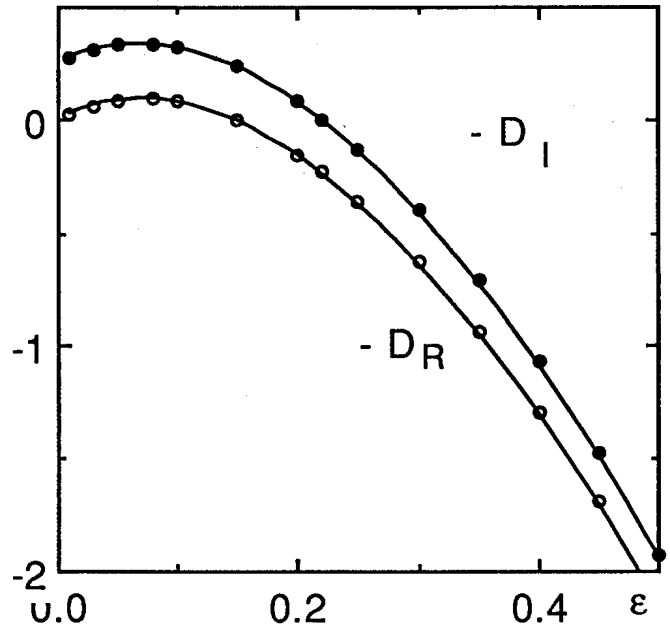

Figure 8 b

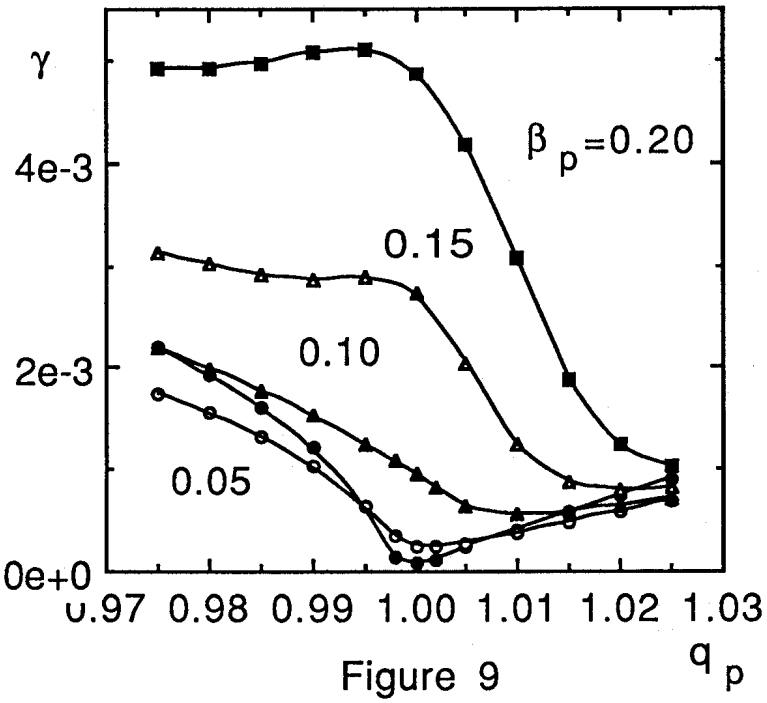

Figure 9

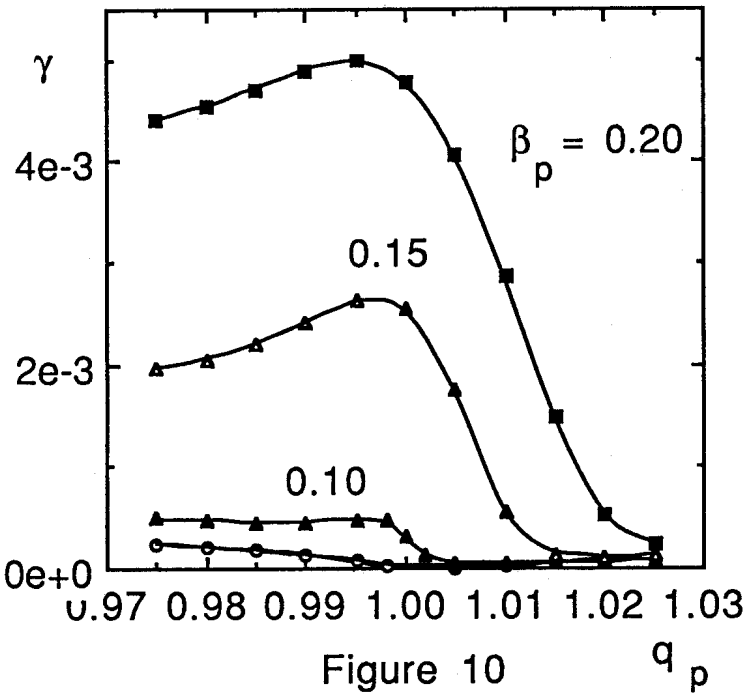

Figure 10

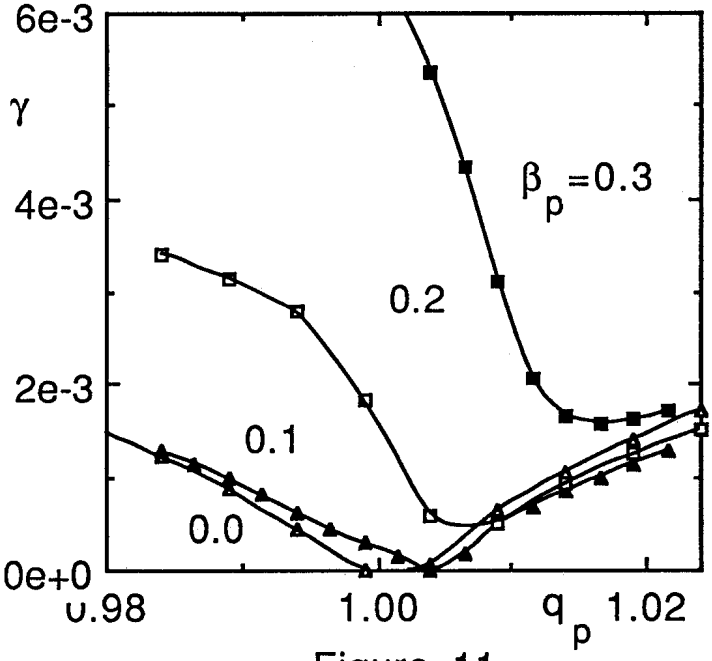

Figure 11

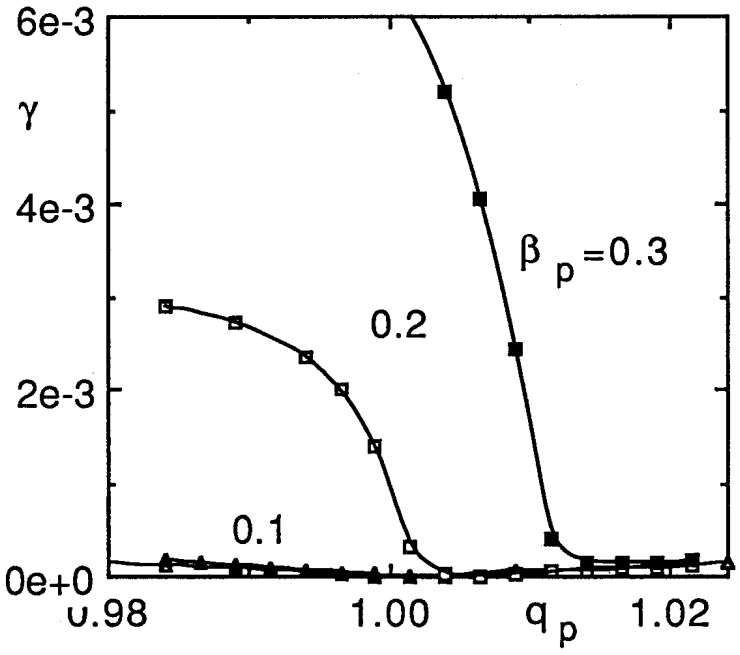

Figure 12

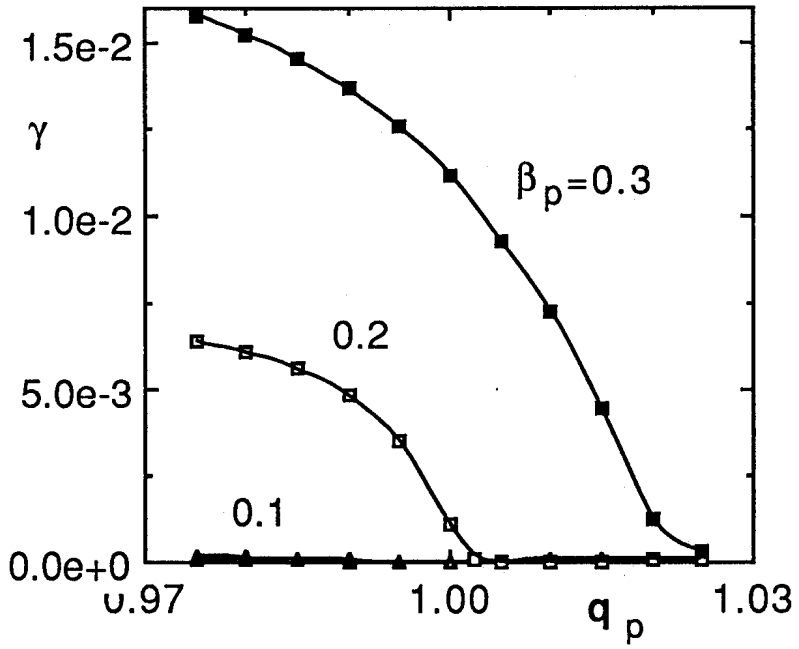

Figure 13a

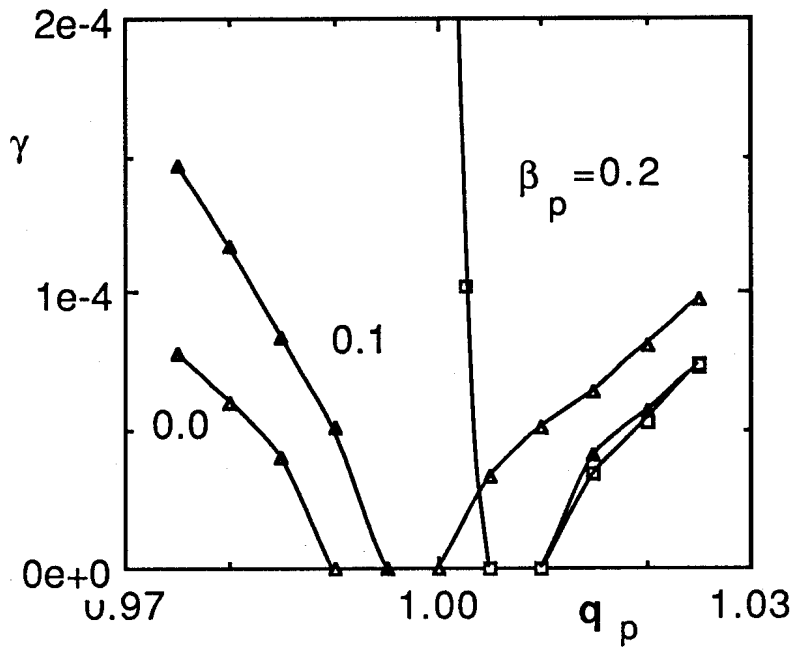

Figure 13b

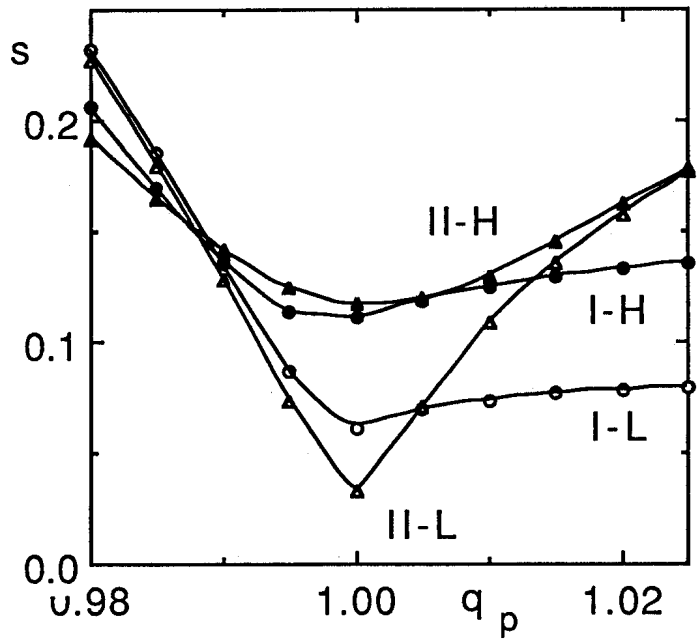

Figure 14

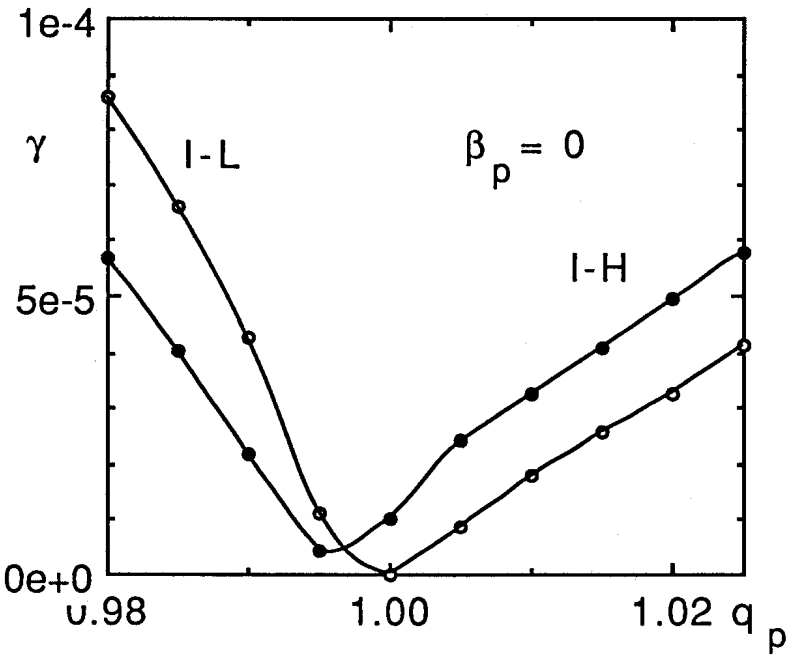

Figure 15 a

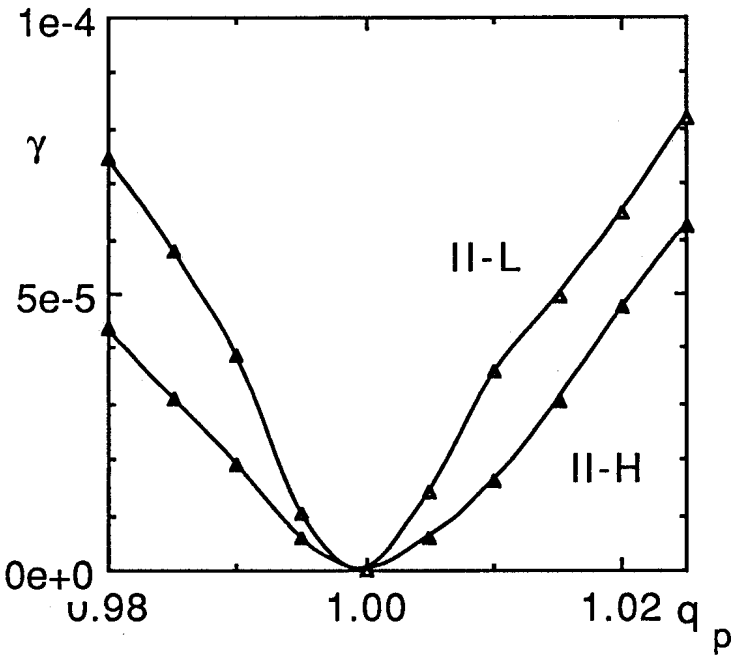

Figure 15 b

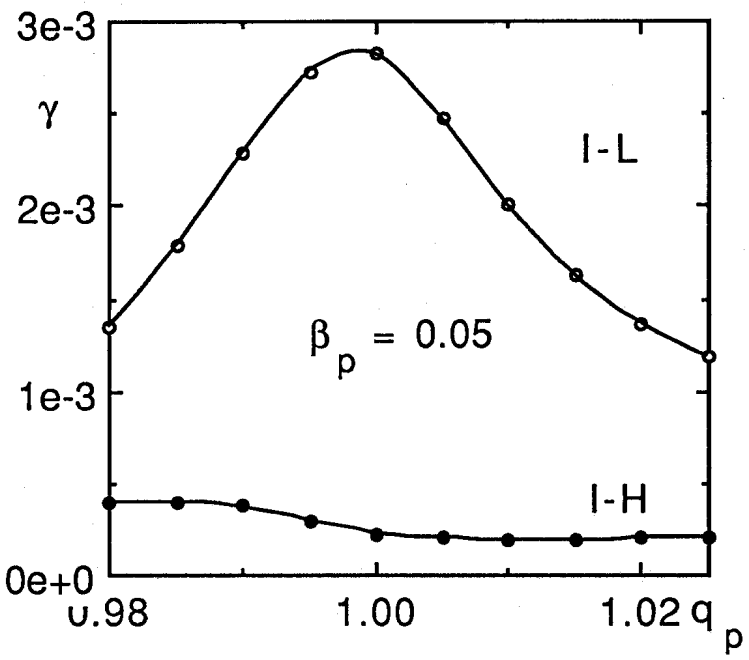

Figure 16 a

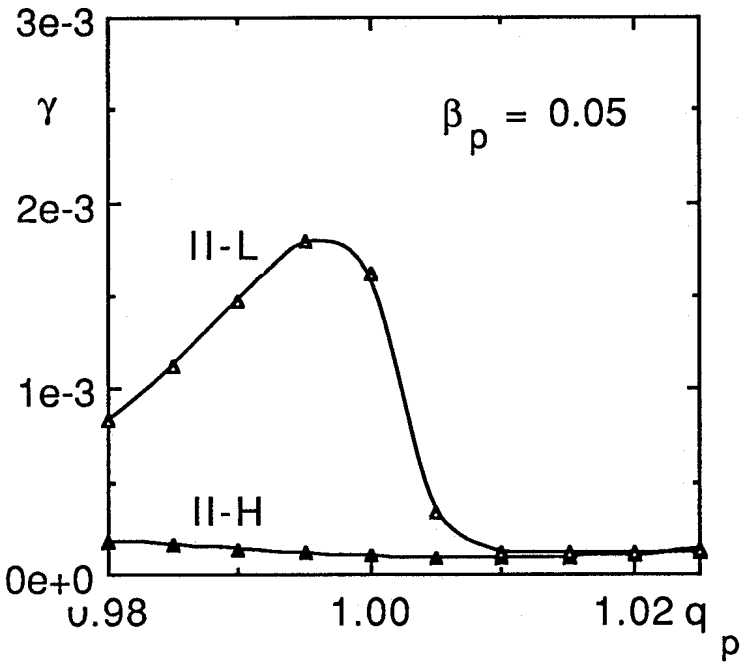

Figure 16 b

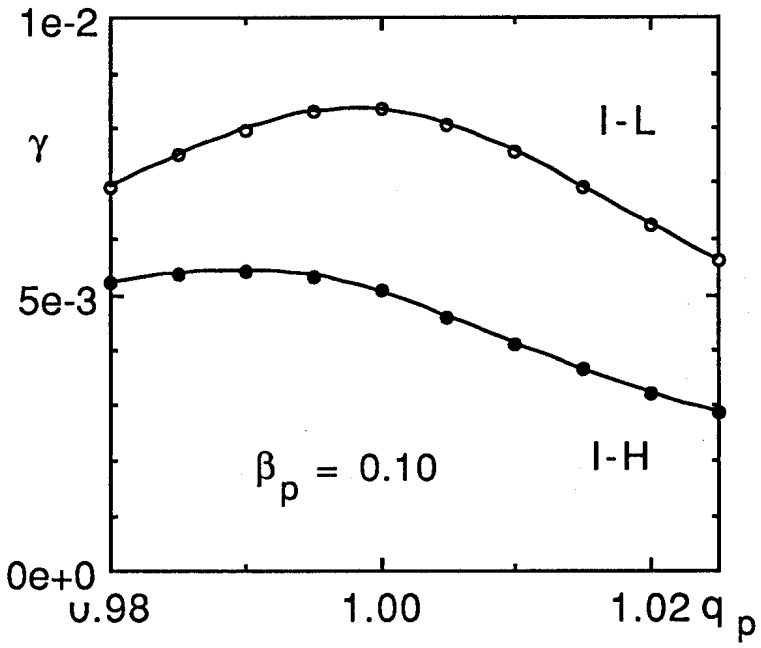

Figure 17 a

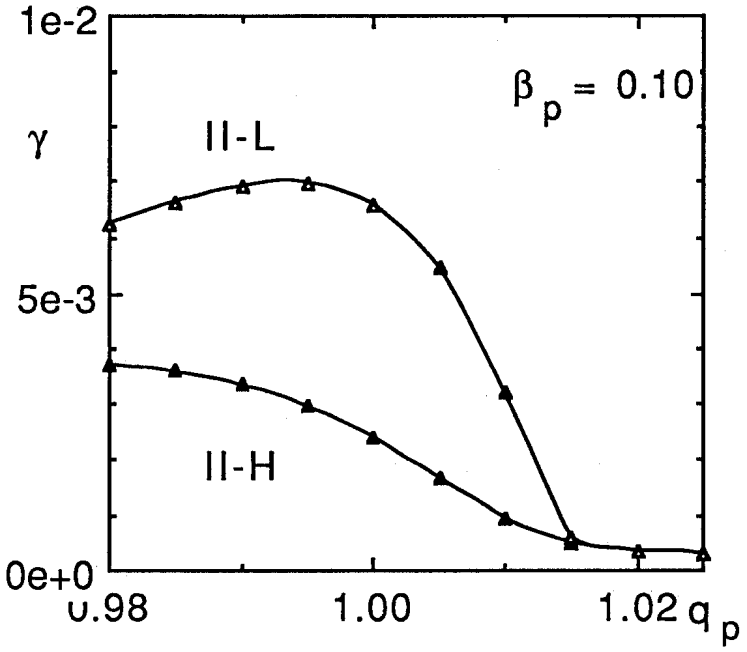

Figure 17 b

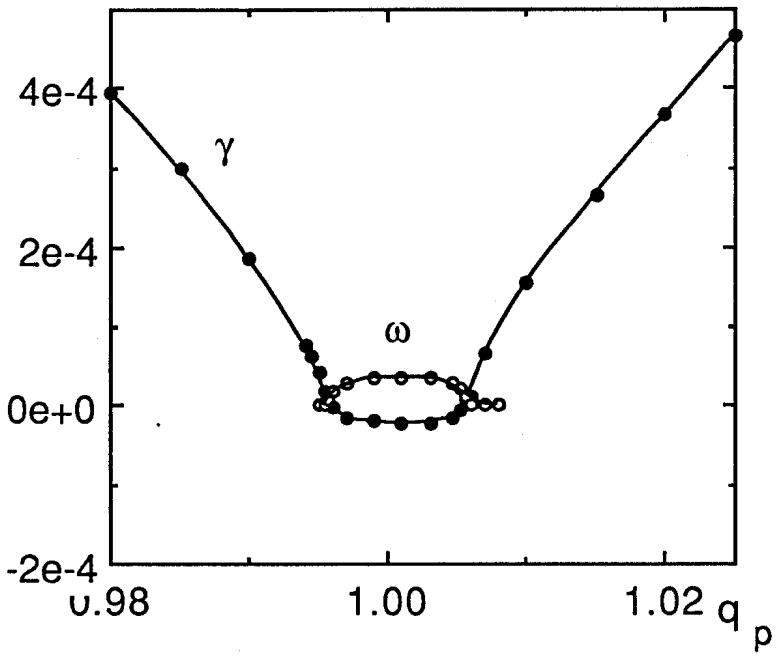

Figure 18